# Super-efficient 3D Pin-wise Reactor Core Analysis by the HCMFD Algorithm

Jaeha Kim and Yonghee Kim
*Korea Advanced Institute of Science and Technology (KAIST), 291 Daehak-ro, Yuseong-gu, Daejeon, Korea, 34141*
**Corresponding author: yongheekim@kaist.ac.kr*

## 1. Introduction

The need of a high-fidelity multi-dimensional core analysis is undeniable since it is essential to estimate the detailed parameters of a reactor core for the core design and safety assessment. Conventionally, the pin-power reconstruction method with an assembly-wise nodal analysis has widely been used for a pin-level analysis of the PWR cores despite of the limited accuracy, since a direct pin-by-pin whole-core analysis is so time-consuming regardless of the methodology used for it.

It is obvious that the accuracy of the whole-core transport analysis is promising, but it still has a long way to go to be utilized easily and quickly due to the massive computing costs. Meanwhile, the pin-by-pin diffusion analysis, which may provide a bit less accurate solutions than by the transport analysis, can now possibly be performed within a reasonably short computing time. Also in the aspect of the accuracy, since there have been continuous efforts, there are many ways suggested to generate nice pin-wise constants so that one can expect an accurate pin-level solution for a whole core.

With expecting that the accuracy of the pin-level diffusion analysis will closely approach to that of the transport analysis soon, the HCMFD (Hybrid Coarse-Mesh Finite Difference) algorithm has recently been developed, which is a combination of two CMFD (Coarse-Mesh Finite Difference) accelerations with the Nodal Expansion Method (NEM) applied on pin-level. [1-3] In the HCMFD framework, the whole-core pin-by-pin analysis can effectively be performed by an efficient parallel computing in a local-global non-linear iterative scheme. In previous studies on the HCMFD method, its feasibility was evaluated only in a 2-D scheme. In this paper, the detailed features of the 3D HCMFD algorithm and some numerical results are presented.

## 2. The HCMFD Algorithm

In the HCMFD algorithm, two CMFD methods are nonlinearly coupled for an iterative local-global strategy, as shown in Fig. 1. The solution of the global eigenvalue problem, represented by Eq. (1), is provided by the one-node CMFD method [4] and it is used to prepare the constraints and boundary conditions of the local problems: the fixed fission source and incoming currents on the boundary.

$$A_{cmfd}^{global}\Phi_{cmfd}^{global}=\frac{1}{k}F_{cmfd}^{global}\Phi_{cmfd}^{global}, \quad (1)$$

$\Phi_{cmfd}^{global}$ : global node-averaged fluxes,
$A_{cmfd}^{global}$ : global system matrix,
$F_{cmfd}^{global}$ : global fission source operator,
$k$ : multiplication factor.

At the same time, the local fixed source problems, represented by Eq. (2), are solved by the conventional two-node CMFD method based on NEM, with the given fixed source and incoming current boundary conditions.

$$M_i^{local}\phi_i^{local}=S_i^{local}, i=1,2,...N, \quad (2)$$

$\phi_i^{local}$ : $i$-th node local fluxes,
$M_i^{local}$ : $i$-th node local system matrix,
$S_i^{local}$ : $i$-th node local fixed source.

The solutions of the local problems are used to calculate both homogenized group constants and reference coarse-mesh interface quantities to generate the correction factors for the global one-node CMFD operators so that the eventual solution of the global problem is equivalent to a pin-level nodal analysis.

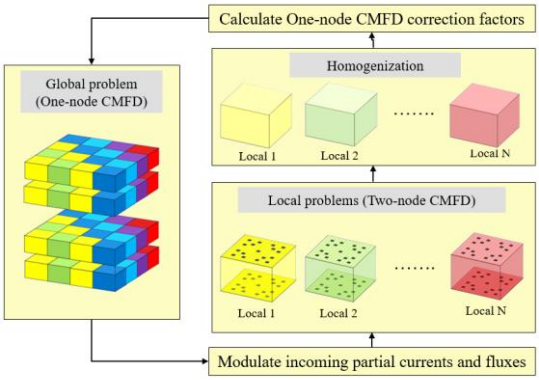


Fig. 1. Schematic diagram of the HCMFD algorithm

In the x-y plane, each single fuel assembly is simply treated as a coarse mesh in the global one-node CMFD, while the pin cells are the fine meshes in each local problem. Unlike in the 2-D case, the size of the axial (z-directional) meshes in both global and local problems can flexibly be determined so that it can possibly be much larger than the fine mesh size in the x-y directions. For this reason, the aspect ratio of a 3-D node can be very far from unity in 3-D applications of the HCMFD algorithm. As in the 2-D scheme, the standard NEM based on the 4th-order polynomials is used for all directions including axial direction in this work.

### *2.1 One-Node CMFD for Global Eigenvalue Problem*

As in Fig. 2, two corrections factors are introduced for each interface in the one-node CMFD method. The two correction factors are determined with Eqs. (3) and (4) using the reference surface flux and net current, and they are implemented in the global net current formulation as in Eq. (5) to preserve the reference higher-order surface-average information. In this case, the reference surface-

averaged flux and net current are calculated by taking the average of the quantities obtained from local fine-mesh NEM calculations.

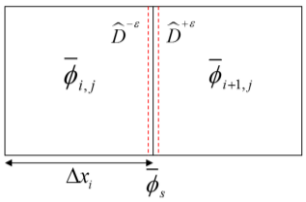


Fig. 2. Inner interface in one-node CMFD

$$\hat{D}^{-\varepsilon} = -\frac{\Delta x \cdot \bar{J}_s^{ref} + 2D_i(\bar{\phi}_s^{ref} - \bar{\phi}_i)}{2(\bar{\phi}_s^{ref} + \bar{\phi}_i)}, \quad (3)$$

$$\hat{D}^{+\varepsilon} = -\frac{\Delta x \cdot \bar{J}_s^{ref} + 2D_{i+1}(\bar{\phi}_{i+1} - \bar{\phi}_s^{ref})}{2(\bar{\phi}_s^{ref} + \bar{\phi}_{i+1})}, \quad (4)$$

$$\bar{J}_s = \frac{2}{\Delta x}\frac{\left(D_i - \hat{D}^{-\varepsilon}\right)\left(D_{i+1} - \hat{D}^{+\varepsilon}\right)}{\left(D_i + D_{i+1} + \hat{D}^{-\varepsilon} - \hat{D}^{+\varepsilon}\right)}\bar{\phi}_i - \frac{2}{\Delta x}\frac{\left(D_i + \hat{D}^{-\varepsilon}\right)\left(D_{i+1} + \hat{D}^{+\varepsilon}\right)}{\left(D_i + D_{i+1} + \hat{D}^{-\varepsilon} - \hat{D}^{+\varepsilon}\right)}\bar{\phi}_{i+1}, \quad (5)$$

*2.2 Two-Node CMFD for Local Fixed-Source Problem*

In the conventional two-node CMFD, only one correction factor is introduced for each interface as depicted in Fig. 3 to preserve the net current. The correction factor is determined using reference net currents as in Eqs. (6) and (7) where the reference net currents are estimated by a pin-level NEM calculation. Then it is used in the net current formulation in Eq. (8) to preserve the reference net current.

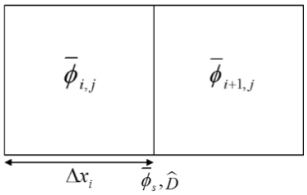


Fig. 3. Inner interface in two-node CMFD

$$\hat{D}_{ii+1} = \frac{-\tilde{D}_{ii+1}(\bar{\phi}_{i+1} - \bar{\phi}_i) - \bar{J}_{ii+1}^{ref}}{(\bar{\phi}_{i+1} + \bar{\phi}_i)}, \quad (6)$$

$$\tilde{D}_{ii+1} = 2\frac{D_i}{\Delta x_i}\frac{D_{i+1}}{\Delta x_{i+1}} / \left(\frac{D_i}{\Delta x_i} + \frac{D_{i+1}}{\Delta x_{i+1}}\right), \quad (7)$$

$$\bar{J}_{ii+1} = -\tilde{D}_{ii+1}(\bar{\phi}_{i+1} - \bar{\phi}_i) - \hat{D}_{ii+1}(\bar{\phi}_{i+1} + \bar{\phi}_i), \quad (8)$$

Since the local problems are fixed-source problems, the incoming partial currents are given on the boundary. The correction factors and corrected net currents on the boundary, especially for the right-end boundary, are expressed as in Eqs. (9) and (10). Those for the left-end boundary can similarly be obtained. In 3D HCMFD, this process is repeated for all 3 directions.

$$\hat{D}_{i,right} = \frac{2D_i\bar{\phi}_i - (\Delta x_i + 4D_i)\bar{J}_s^{ref} - 8D_i\bar{J}^-}{2\bar{\phi}_i + 4\bar{J}_s^{ref} + 8\bar{J}^-}, \quad (9)$$

$$\bar{J}_{s,right} = \frac{2(D_i - \hat{D}_i)}{\Delta x_i + 4(D_i + \hat{D}_i)}\bar{\phi}_i + \frac{-8(D_i + \hat{D}_i)}{\Delta x_i + 4(D_i + \hat{D}_i)}\bar{J}^-, \quad (10)$$

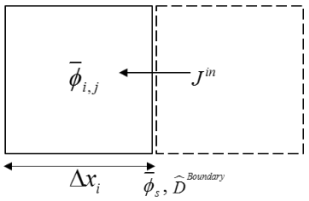


Fig. 4. Right-end boundary in two-node CMFD

Basically, the global node balance is implemented to each local problem in terms of the modulated fluxes and also the modulated incoming partial currents on the boundary as boundary conditions. For a better convergence, the local two-node CMFD calculation is performed twice per one local analysis with an overall exchange of the partial currents and the transverse leakages between the local problems. In this way, the newest high-order quantities estimated by solving each local problem can be quickly reflected in neighboring local problems, and the convergence can be accelerated and also the possible numerical instability at the early stage of the local-global iteration can be eliminated.

*2.3 Nodal Expansion Method in Local Problems*

In the two-node CMFD acceleration scheme based on NEM, the reference net currents on every inner interfaces are estimated by NEM with neighboring two nodes. For each node and each group, the detailed 1-D fluxes are expanded by the 4-th order polynomial basis functions. The 2-nd order transverse leakage terms are pre-estimated using the node-averaged transverse leakage values in three sequential nodes. In this study, the matrix equations for obtaining the expansion coefficients are solved by utilizing the analytic solutions since it is computationally more efficient.

Meanwhile, on the local boundary, there is no neighboring node to be coupled and thus it will be a single-node problem. On the boundary node, the node-averaged transverse leakage in the neighboring node which is outside of the local boundary should also be given since they are not available in each independent local problem. As shown in Fig. 5, there are two kinds of information on each boundary surface which should be given. Since no information can be exchanged after once the parallel computing for the local problems begins, they are all saved and distributed prior to the local fixed source calculation.

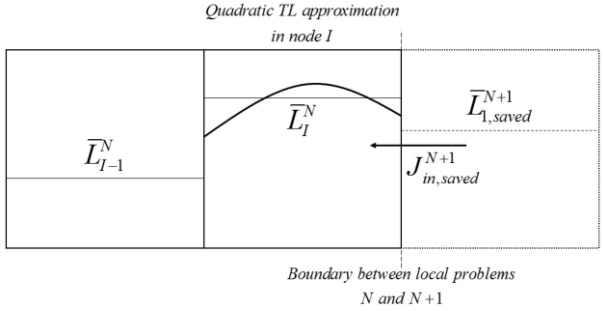


Fig. 5. Information on every local boundary

### 3. Numerical Results

In this work, a 2-D modified EPRI-9R benchmark problem described in Figs. 6 and 7 was simply extended to a 3-D problem as shown in Fig. 8. The active core height is set to be 200cm with upper and lower 20cm reflector layers, and coarse mesh size in z-direction is basically 20cm. In order to see impacts of control rod position, two cases were considered in this study, one with the central control rod fully inserted (Case 1), and the other case with the control rod inserted to the mid-plane of the active core (Case 2).

The convergence criterion for both fission source and eigenvalue was $10^{-7}$, and the local and global problems were both solved by a BiCGSTAB (Biconjugate gradient stabilized) method [5]. The local analysis was performed every 10 global outer iterations, which is an optimized number in terms of computing time for the two 3-D cases. All calculations were performed on Intel Xeon E5-2697 v3 2.60 GHz CPU with 28 physical cores. In this study, the parallel computing was performed using the OpenMP parallel algorithm. [6]

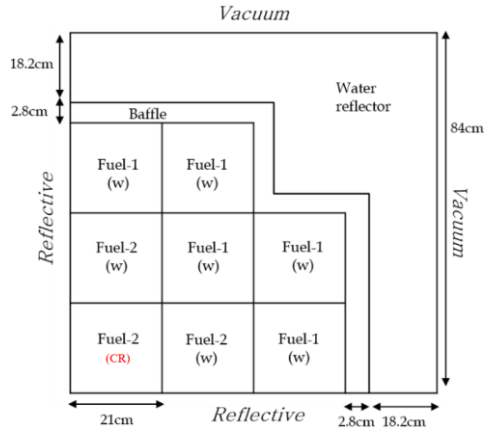


Fig. 6. 2-D modified EPRI-9R benchmark problem

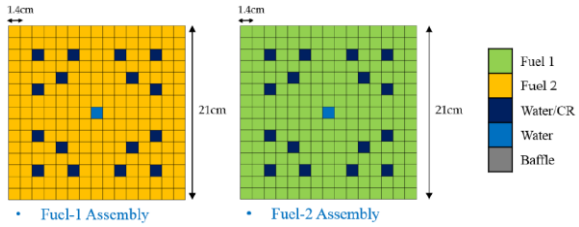


Fig. 7. EPRI-9 fuel assemblies

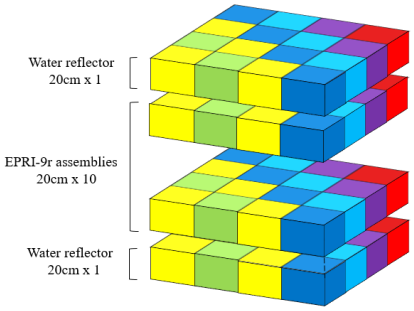


Fig. 8. 3-D extension of EPRI-9R benchmark problem

First, the parallelizable portion of the whole computational loads, the so-called parallelism, depending on the axial partition was briefly analyzed in Case 1 and the results are given in Table I. Even with the minimum axial partition with a 20 cm coarse mesh size, the parallelism is 99.35%, and it further increases to 99.90% when the number of axial nodes is increased by a factor of 10. Table I indicates that the parallel computational efficiency of the 3D HCMFD algorithm can be very high.

Table I. Parallelism in Case 1

| Method | Mesh size (cm) | Parallelism (%) |
|---|---|---|
| HCMFD | 1.4 x 1.4 x 20 | 99.35 |
| HCMFD | 1.4 x 1.4 x 2 | 99.90 |

To investigate the numerical performances depending on the number of axial layers in local problems, two benchmarks were solved with various axial divisions as shown in Tables II and III. First, the comparison of the accuracy of solutions depending on the axial mesh refinement in local problems is given in Table II. For comparison, fine-mesh FDM solutions are also included, but it should be noted that they cannot be true references since the mesh size for FDM is not small enough. In this work, the k-eff values by HCMFD with 10 axial layers were chosen as reference values.

Table II. Impacts of axial mesh size on k-eff

| Case | Method | Axial layers | Mesh size (cm) | k-eff | Error (pcm) |
|---|---|---|---|---|---|
| 1 | HCMFD | 1 | 1.4x1.4x20 | 0.881055 | -2.4 |
| 1 | HCMFD | 2 | 1.4x1.4x10 | 0.881077 | -0.2 |
| 1 | HCMFD | 10 | 1.4x1.4x2 | 0.881079 | Ref. |
| 1 | FDM | 10 | 0.2x0.2x2 | 0.881083 | +0.4 |
| 2 | HCMFD | 1 | 1.4x1.4x20 | 0.905878 | +16.4 |
| 2 | HCMFD | 2 | 1.4x1.4x10 | 0.905757 | +5.7 |
| 2 | HCMFD | 4 | 1.4x1.4x5 | 0.905714 | +1.2 |
| 2 | HCMFD | 10 | 1.4x1.4x2 | 0.905702 | Ref. |
| 2 | FDM | 10 | 0.2x0.2x2 | 0.905650 | -5.2 |

In Table II, one can note that the axial mesh refinement results in a converged solution for the two cases. For the 1st benchmark (Case 1), a coarse mesh (10~20cm) NEM can provide accurate solutions, while the solution is more sensitive to the axial mesh size in Case 2. This is because the axial flux profile is rather smooth in Case 1 and it is strongly position-dependent due to the partial insertion of the control rod in Case 2. In the case of high axial heterogeneity, the axial mesh size for the NEM should be rather small, 5~10 cm, for an accurate solution.

Table III shows the parallel computational efficiency depending on the number of cores and the axial divisions in local problems. While the parallel computational efficiency decreases as the number of cores increases, the efficiency was slightly higher with more axial layers per local problem since the parallelism increases as the axial

divisions increase. It is expected that the parallel computational efficiency can be improved by further optimization in utilizing the OpenMP parallel algorithm.

Table III. Parallel computational efficiency in Case 1

| No. of core | Axial layers per local problem | CPU time (sec) | Speed-up | Efficiency (%) |
|---|---|---|---|---|
| 1 | 1 | 8.75 | - | -- |
| 2 | 1 | 4.55 | 1.92 | 96.15 |
| 5 | 1 | 2.05 | 4.27 | 85.37 |
| 10 | 1 | 1.26 | 6.94 | 69.44 |
| 20 | 1 | 0.82 | 10.67 | 53.35 |
| 1 | 4 | 57.17 | - | -- |
| 2 | 4 | 29.47 | 1.94 | 97.00 |
| 5 | 4 | 12.90 | 4.43 | 88.64 |
| 10 | 4 | 7.64 | 7.48 | 74.83 |
| 20 | 4 | 5.37 | 10.65 | 53.23 |

Additionally, by the inborn characteristics of the HCMFD, one can easily set the degrees of the axial mesh refinement in a layer-by-layer sense. Basically, to obtain a reasonably accurate solution, a coarse axial mesh is enough in an axially-homogeneous geometry, like in the Case 1 benchmark, while a bit finer mesh is required when there is a strong axial heterogeneity. When treating a problem with a local axial heterogeneity as in Case 2, a regional mesh refinement can be very useful to reduce the computing time. In the HCMFD algorithm, a regional axial mesh refinement is a simple work since the local mesh refinement is separately done after defining the global coarse meshes.

Actually, in the 3D HCMFD algorithm, one can flexibly determine the eventual z-directional mesh size in two steps, by adjusting the coarse mesh size itself or by refining the local mesh size in coarse-mesh local problems. After some tests on the impact of each approach on the accuracy and computing time, we found that the refinement of the local mesh size with a uniform coarse mesh size is a more favorable approach. For this reason, only the local refinement with fixed coarse axial mesh (20cm) was considered for some detailed analysis regarding the regional mesh refinement in this study.

Table V. Regional axial mesh refinement in Case 2

| Global Layer # | Regional Axial Mesh Refinement | | | |
|---|---|---|---|---|
| | #1 | #2 | #2 | #3 |
| 1 | 1 | 4 | 1 | 2 |
| 2-5 | 1 | 4 | 1 | 1 |
| 6-7 | 1 | 4 | 4 | 4 |
| 8-11 | 1 | 4 | 1 | 1 |
| 12 | 1 | 4 | 1 | 2 |
| k-eff | 0.905878 | 0.905714 | 0.905660 | 0.905700 |
| Error (pcm) | +16.4 | +1.2 | -4.2 | -0.2 |
| CPU time (sec) | 9.41 | 49.39 | 16.08 | 18.15 |

In Table V, refinement #1 and #2 are the uniformly refined cases as already presented in Table II, while #3 and #4 are locally-refined ones. In #3, the regional axial mesh refinement is only applied near the tip of the control rods, while the axial reflector regions are additionally refined in #4. By using a regional refinement only near the control rod tip, the k-eff error was dramatically decreased from 16.4 pcm to 4.2 pcm, and it was further decreased to 0.2 pcm by the additional refinement in axial reflector regions. The single-core computing times in refinement #3 and #4 were about one third of that in #2, the uniformly refined case.

## 4. Conclusions

The HCMFD algorithm was successfully extended to a 3-D core analysis without any numerical instability though the aspect ratio of the node shape is very far from unity. We have shown that 3-D pin-wise core analysis can be done very effectively with the HCMFD framework due to its inherent characteristics. Additionally, it was demonstrated that parallel efficiency of the new 3D HCMFD scheme can be quite high on a simple OpenMP parallel architecture. It is concluded that the 3D HCMFD will enable an efficient pin-wise 3-D core analysis.

## ACKNOWLEDGMENTS

This work was supported by the National Research Foundation of Korea (NRF) Grant funded by the Korean Government (MSIP) (NRF-2016R1A5A1013919).

## REFERENCES

[1] Seongho Song, Hwanyeal Yu, and Yonghee Kim, "An Efficient One-Node and Two-Node Hybrid CMFD method," *Proceedings of the Korean Nuclear Society Autumn Meeting*, Gyeongju, South Korea, October 29-30, 2015.

[2] Seongho Song, Hwanyeal Yu, and Yonghee Kim, "Pin-by-Pin Reactor Core Analysis Based on a NEM-based Two-level Hybrid CMFD Algorithm," *Proceedings of PHYSOR 2016*, Sun Valley, Idaho, USA, May 1-5, 2016.

[3] Seongho Song, Hwanyeal Yu, and Yonghee Kim, "Pin-by-Pin Core Calculation with an NEM-Based Two-Level Hybrid CMFD Algorithm," *Transactions of ANS 2016*, New Orleans, USA, June 12-16, 2016.

[4] H. C. Shin and Y. Kim,"A Nonlinear Combination of CMFD (Coarse-Mesh Finite Difference) and FMFD (Fine-Mesh Finite Difference) Methods, *Proceedings of Korean Nuclear Society Spring Meeting*, Pohang, Korea, May, 1999.

[5] H.A. Van Der Vorst, "Bi-CGSTAB: A Fast and Smoothly Converging Variant of Bi-CG for the Solution of Nonsymmetric Linear Systems", *SIAM J. Sci. and Stat. Comput.*, 13(2), 631–644, 1991.

[6] OpenMP API, "OpenMP Application Program Interface", Version 4.0, July, 2013.